



Insight into Atomic-Scale Adhesion at the C–Cu Interface During the Initial Stage of Nanoindentation

Jian Gao¹ · Xichun Luo¹ · Wenlong Chang¹ · Zhengjian Wang¹ · Yongda Yan² · Yanquan Geng²

Received: 31 December 2021 / Revised: 2 August 2022 / Accepted: 3 August 2022
© The Author(s) 2022

Abstract

Adhesion is a common phenomenon in nanomachining which affects processing accuracy and repeatability. As material removal approaches the atomic or close-to-atomic scale, quantum mechanics becomes the dominant principle behind the atomic-level interaction. However, atomic-scale effects cannot be properly described by empirical potential function-based molecular dynamics simulations. This study uses a first-principles method to reveal the atomic-scale adhesion between a diamond tip and a copper slab during initial-stage nanoindentation. Using a simplified tip and slab model, adhesion energy, electronic distribution, and density of states are analyzed based on quantum chemistry calculation. Results show that atomic adhesion is primarily due to the covalent bonding interaction between C and Cu atoms, which can induce structural changes to the diamond tip and copper slab. The effects of tip position and angles on adhesion are further studied through a series of simulations. The results show that adhesion between the tip and slab is sensitive to the lattice structure and a variant in angstroms is enough to cause different adhesion and structural changes. The actual determinants of adhesion can only be the atomic and electronic structures at the tip–slab interface. Bond rotation and breakage are observed during simulation and their effects on adhesion are further discussed. To conclude, the first-principles method is important for the analysis of an atomic-scale interaction system, even if only as an aid to describing adhesion at atomic and electronic scales.

Keywords Nanoindentation · Adhesion · Diamond · Copper · First-principles · Density functional theory

1 Introduction

Atomic and close-to-atomic scale manufacturing (ACSM) or Manufacturing III aims to manufacture atomic or close-to-atomic scale patterns with atomic-level accuracy through removal, addition, or migration [1]. Research on ACSM involves the fundamental study, development of process and equipment, and experimental validation to promote the development of next-generation electronic, energy, and medical devices [2].

Compared with other potential lithographic techniques [3], mechanical machining methods can directly pattern material surfaces. Atomic force microscopy (AFM)-based scratching has achieved patterns with feature sizes at

micro- and nanoscales [4, 5]. However, when the patterning reduces to the atomic or close-to-atomic scale, the experiment could be difficult to implement [6]. Thus, the experiments typically require an operation under critical conditions such as ultrahigh vacuum and cryogenic temperature and the use of high-resolution scanning probe microscopy (SPM) to remove or manipulate surface atoms and atomic clusters [4, 7, 8]. However, the challenge lies not only in achieving tool control, sample preparation, and elimination of environmental effects at this scale but also in the fundamental understanding of the atomic-scale tool–work interaction, which is based on quantum theory rather than classical theory [1, 9]. During atomic manipulation or removal, tool sharpness and tool–sample distance or patterns are on a scale of tens of atoms. In this case, quantum mechanical effects are becoming more pronounced, and atomic-scale adhesion, material transfer, bond forming, and breaking cannot be accurately described using classical molecular dynamics simulations that are based on empirical potential functions.

A density functional theory (DFT)-based first-principles method should be used to allow a reliable description of

✉ Xichun Luo
xichun.luo@strath.ac.uk

¹ Centre for Precision Manufacturing, DMEM, University of Strathclyde, Glasgow, UK

² Center for Precision Engineering, Harbin Institute of Technology, Harbin, People's Republic of China

the tool–work interaction. Based on quantum mechanics, this method applies an iterative process to determine the ground state of a system through the optimization of atomic coordinates and distribution of electrons; analysis of processes and results can provide an accurate description of the atomic and electronic behaviors under chemical bonding interactions. Sugimoto et al. [10] revealed the mechanism of lateral manipulation of adatoms on a Si (111)- 7×7 surface through a first-principles study; results showed that the tip–sample interaction could weaken the covalent bonding and reduce atomic diffusion barriers between adjacent sites. Jarvis et al. [11] conducted the first-principles simulation and demonstrated the possibility of using distinct tip apices to achieve the atomic manipulation. Tavazza et al. [12] applied the DFT method to simulate nanoindentation on a Ni surface and revealed a complex material transfer during the process. Tavazza et al. [13] also used the DFT calculation to validate the interaction potential in molecular dynamics simulation of nanoindentation. Sanna et al. [14] modeled the AFM imaging on LiNbO_3 surface within the DFT; the result indicated that the calculation was consistent with experiment, and the contrast mechanism was attributed to the charge accumulation at O atoms. Based on these theoretical studies, the chemical interaction plays a major role in atomic-scale manipulation or removal and quantum mechanics-based simulations are important for the evaluation of the atomic-scale interactions. These simulation studies not only provide a comprehensive understanding of the manufacturing mechanism but also help to explore the atomic-scale frictional behaviors at the interface, all of which are important in addressing the challenges in building next-generation atomic devices [15].

Numerous researchers have investigated the machining of copper using diamond tools using experimental and theoretical methods [16–20]. However, the nature of adhesion and atomic effects have rarely been investigated. In this work, a series of first-principles calculations will be performed to study the initial stage of nanoindentation. This simulation study aims to reveal the tool–work adhesion, which is a common phenomenon that weakens process accuracy and induces tool wear [21–25]. The main discussion focuses on the nature of interaction and the effects of the interface lattice on adhesion. The atomic-scale behavior as bonding and interface reconfiguration will also be analyzed to discuss its possible influence on the nanoindentation results. Through this paper, the authors would like to describe the tool–work interaction down to the electronic scale and provide a comprehensive understanding of the atomic-scale machining mechanism.

2 First-Principles Calculations

In this work, first-principles calculations were carried out on the basis of the DFT using the Quantum ESPRESSO [26, 27]. The exchange–correlation function was calculated using the Perdew–Burke–Ernzerhof (PBE) functional [28]. Pseudopotentials for Cu, C, and H atoms were PBE potentials obtained from the Standard Solid State Pseudopotential library [29], which have been used to reveal basic interfacial bonding features [12, 30–32], as they provide a good balance between accuracy and efficiency. Dispersion interactions are not considered in this work, as they primarily contribute to a long-range background, which could be featureless at the atomic scale [33, 34]; instead, this study focused on adhesion due to strong chemical bonding, which is the leading cause of chemical wear and atomic transfer in tool–work contact [24, 35]. Based on convergence tests shown in Fig. S1, kinetic energy cutoffs of 50 and 500 Ry were used for the calculation of wavefunction and charge density, respectively. Gaussian smearing with a 0.01 Ry spreading value is applied for Brillouin-zone integration. The postprocessing tools of Quantum ESPRESSO and VESTA [36] were used to generate data and figures in this paper.

This work involves a series of first-principles calculations to reveal the atomic and electronic behavior during nanoindentation. We selected a semistatic relaxation approach that has been used in previous research to deal with similar processes and simulate the tip approaching and separating from a surface [12, 37]. In each step, a “relax” calculation will be conducted for the tip–slab ensemble by fixing the bottom Cu atom layer, top C atom layer, and all H atoms. The system will be converged if the total energy change between two consecutive optimizing steps and atomic forces were less than 0.0001 Ry and 0.025 Ry/Bohr, respectively. This process will obtain ground-state energy and relaxed lattice structures. After each relaxation step, the top atom layers in the tip will serve as grips and will be lowered or lifted by 0.2 or 0.3 Å for the next relaxation calculation. In revealing the electronic characteristics of the ensemble, an “scf” calculation was performed on the basis of the coordinates from relaxation to calculate the charge density distribution, and an “nscf” calculation was used with a denser k-point grid for the density of states (DOS).

The determination of the contact area during nanoindentation is a difficult task [38, 39]. The interaction between a diamond tool and a metal sample in the experiment could be complex, and the simulation of the whole system using the first-principles method remains impractical. Based on previous studies [40–44], the initial-stage adhesion was primarily attributed to the interaction between dangling bonds on the tool and surface atoms on the substrate. Therefore, this work adopted a simple and well-defined single-atomic contact

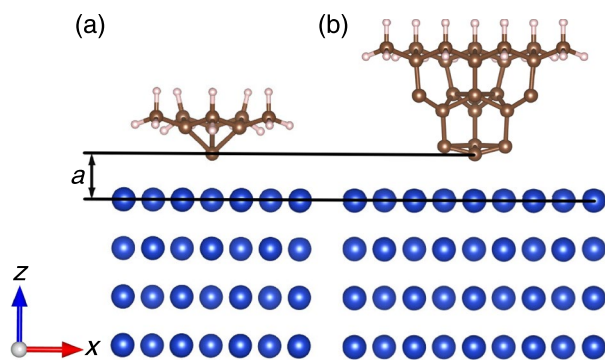


Fig. 1 Schematics of the diamond tip and Cu (111) slab: **a** model I and **b** model II

model (model I) to simulate indentation using an AFM tip (Fig. 1a). The tip model was idealized as a pyramid; that is, only one atom with one dangling bond protruded from the tip; thus, its angular and positional relationship with the surface lattice can be studied. The top carbon atoms at the tip were fixed and saturated with hydrogen atoms. Model II (Fig. 1b) was used for comparison to show the effect of C layers on adhesion. The top three layers of carbon atoms and all hydrogen atoms were fixed. A copper slab with a (111) crystallographic direction on the top surface was used to model the substrate. The periodic boundary conditions were applied to the x , y , and z directions. Along the z direction, a vacuum gap of 15 Å separated slabs to avoid interactions among periodic cells. In addition, a simple four-layer slab model was used for the substrate to describe initial-stage nanoindentation, and the dimensions of models I and II were $7.68186 \text{ \AA} \times 8.87024 \text{ \AA} \times 6.27221 \text{ \AA}$ and $10.242479 \text{ \AA} \times 8.87024 \text{ \AA} \times 6.27221 \text{ \AA}$, respectively, corresponding to k -point grids of $5 \times 4 \times 1$ and $4 \times 4 \times 1$ for sampling in the Brillouin region [45], which have been proven to reach energy convergence (Fig. S2). The Cu atoms in the bottom layer were fixed to prevent the overall z -direction movement. Before the assembly of the diamond tip and copper slab, the tip and slab were relaxed separately to isolate the effects of self-relaxation on the tip–slab interaction.

3 Nature of Adhesion

We conducted a series of first-principles calculations to reveal the details of the lattice structure, charge distribution, and DOS, and describe the nature of the interaction between the diamond tip and copper slab. For model I, the tip was placed on the top site at a distance of 3 Å from the surface.

First, relaxation was conducted for the ensemble to obtain the optimized atomic coordinates with the lowest total energy. Then, a self-consistent calculation was used to examine the electronic distribution. Here we used a charge density

difference (CDD) to demonstrate the electronic redistribution under the interaction, further reflecting the formation mechanism of the bond. The CDD of the tip–slab ensemble was calculated as follows:

$$\Delta\rho = \rho_{\text{tip+slab}} - (\rho_{\text{tip}} + \rho_{\text{slab}}) \quad (1)$$

where ρ_{tip} and ρ_{slab} are the charge densities of the isolated tip and slab, respectively; $\rho_{\text{tip+slab}}$ is the charge density of the tip–slab system. The CDDs were visualized as isosurfaces which divided the space into yellow and blue regions (Fig. 2a). The yellow region represents the electron gain and the blue region represents the electron loss. The apparent electron loss appears around atom 2. The electron gain between the tip apex and slab surface reaches its maximum, indicating covalent characteristics; that is, the electron gain region is shared by two atoms. In addition, the electron gain (yellow) region is not evenly shared by the two atoms, but is closer to atom 1 than to atom 2. Therefore, the electron affinity of tip atom 1 is better than that of atom 2.

For a more comprehensive understanding of the electronic characteristics, the projected density of states (PDOS) for atoms at the interface was calculated, and the result is shown in Fig. 2b, which shows the electronic distribution in every orbit. By contrast, an apparent hybridization of $2p$ orbital on atom 1 and $3d$ orbital on atom 2 was observed near the Fermi level, indicating the formation of a covalent bond between atoms 1 and 2.

The C–Cu interface attraction was derived from covalent bonding; thus, the presence of unpaired p electrons on the diamond and unpaired d electrons on copper was essential for the formation of a strong attraction at the C–Cu interface. This conclusion is consistent with previous studies [31, 46]. When the tip approached the surface at a distance, the unpaired electron on the apex would attract d orbital electrons on the copper surface to form a pair. This finding indicates the strong adhesion at the C–Cu interface from the electronic scale. However, the C–Cu covalent bonding tended to be weak because atom 2 can only provide less than one valence electron to form a covalent bond because each Cu atom has only one valence electron, which is involved in forming a covalent bond while maintaining metallic bonds with its neighboring Cu atoms.

4 Nanoindentation on the Copper Surface

4.1 Adhesion Energy

In this work, the adhesion strength was evaluated on the basis of the adhesion energy E_{ad} , which represents the energy required to separate the tip from the slab neglecting plastic lattice changes and atomic diffusion. The equation is given as follows:

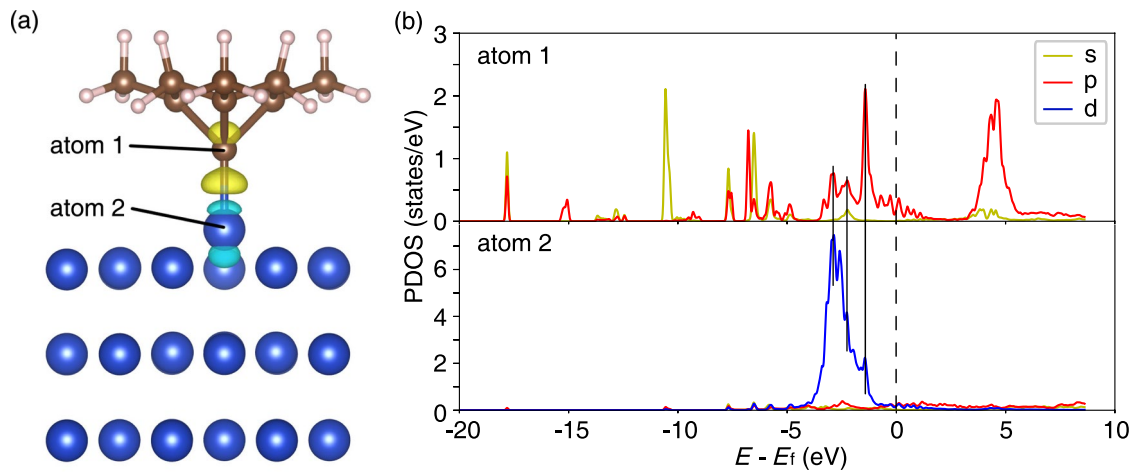


Fig. 2 CDD and PDOSs for model I with a distance of 3 Å on the top site; **a** CDD, plotted with isosurface level of 0.01; **b** DOS for atom 1 projected on 2p orbitals and atom 2 projected on 3d orbitals. E_f is the Fermi energy

$$E_{\text{ad}} = (E_{\text{tip}} + E_{\text{slab}}) - E_{\text{tip+slab}} \quad (2)$$

where E_{tip} and E_{slab} are the total energies of the isolated tip and slab, respectively. $E_{\text{tip+slab}}$ is the total energy of the tip–slab ensemble.

4.2 Positional Relationship Between the Tip and Slab

Vertically, the tip–slab distance is defined as the distance from the spherical center of the apex atom to the central plane of surface atoms (Fig. 1), without considering the structural changes under the tip–slab interaction. Therefore, the apex atom will be coplanar with the surface atoms at a distance of 0 Å in the absence of tip–slab interactions. This study only focuses on the interaction when the tip and slab

are almost or just in a contact state, with a distance between 1.1 and 4.1 Å, to emphasize the effects caused by adhesion.

Horizontally, various sites are identified on the (111) surfaces of bulk FCC copper. Along the z direction, atomic layers are stacked in the order of “ABCABC”. Thus, three high-symmetry sites are found (Fig. 3a). The top site is right atop a surface atom. The fcc and hcp sites are equidistant from the three nearest Cu atoms on the surface, but the fcc site is right above a Cu atom in the third layer and the hcp site is right above a Cu atom in the second layer.

Model I, which was used in this work, aims to describe the single-atomic contact at the interface, but the angular relationship between the tip and surface lattice must be considered in the simulation. Based on the atomic coordinates at the tip–slab interface, the effect of tip angle on adhesion could be particularly apparent when the tip is placed at the fcc and hcp sites on the surface. Considering the tip as an

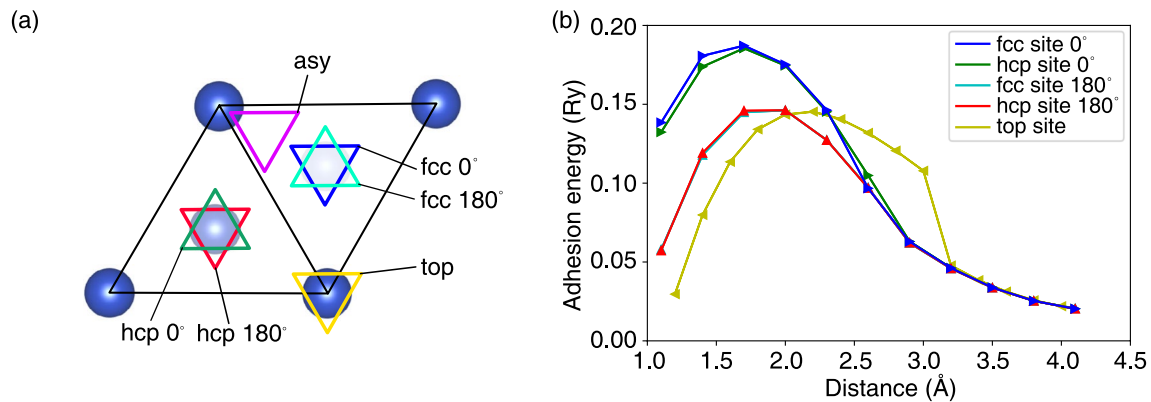


Fig. 3 **a** Schematic top view of the fcc copper unit in the (111) surface. Triangles with different colors represent the positions of the tip on the surface. **b** Influence of tip–slab distances on adhesion energies

for model I on fcc and hcp sites with angles of 0° and 180°, and on the top site during indentation on the Cu (111) surface

inverted triangular pyramid with an equilateral triangular base, each site has two angular relationships corresponding to angles of 0° and 180° to the fcc and hcp sites. The positional relationship between the tip and slab is shown in Fig. 3a.

4.3 Adhesion for the Tip on High-Symmetry Sites

A series of simulations were performed corresponding to the positional relationships is shown in Fig. 3a. The tip was placed accordingly to perform semistatic indentation. The top-layer C atoms and all H atoms served as grips, which could be lowered at each step. The adhesion energies at different distances are illustrated in Fig. 3b.

Figure 3b shows that the adhesion energies on all sites increase to a maximum at certain distances and then decrease as the tip approaches the surface from 4.1 to 1.1 Å. Among these sites, the maximum adhesion energies seem to appear at a distance of 1.7 Å when the angles are at 0° to the target lattice sites. Through comparison, we can see that the hcp and fcc sites did not significantly affect their attraction to the approaching tip, whereas their relative angular relationship to the tip could cause different adhesion energies. When the distance was between 1.1 and 2.8 Å, the tip adhesion at 0° was stronger than that at 180° . This result is due to the difference in lattice structures at the tip–slab interface, which indicates that the tip positioned at 0° to the

target lattice has a more stable equilibrium configuration and exhibits higher adhesion energy. These results present the interaction between the diamond tip and the Cu (111) surface. Therefore, the tip's relative angles to the lattice will affect adhesion, which causes a difference in the lattice structure.

For the tip on the top site, the adhesion effect was evident as the tip approached the surface at a distance of 3 Å. This finding was demonstrated by the fact that a Cu atom was raised above the surface and accompanied by a rapid increase in tip–slab adhesion energy. This effect led to the strongest adhesion among all high-symmetry sites at this distance because of the formation of a covalent bond when a Cu atom (atom 2 in Fig. 2a) jumped to contact with the apex atom under the interaction. Among the high-symmetry sites on Cu (111) surface, the atomic jump only occurred on the top site. Our simulation also showed that a different threshold of force or energy would lead to some variation in the distance at which the atomic jump occurs, but atomic jumps could only occur during indentation on the top site and visibly affect the adhesion.

Through the analysis on CDDs and C–Cu bond lengths for the tip–slab ensemble at different distances (Fig. 4), we can describe the tip indentation on the top site of the Cu (111) surface. When the distance was larger than the atomic jump distance (3 Å), the tip–sample interaction was weak; thus, no significant atomic displacement occurred. As the

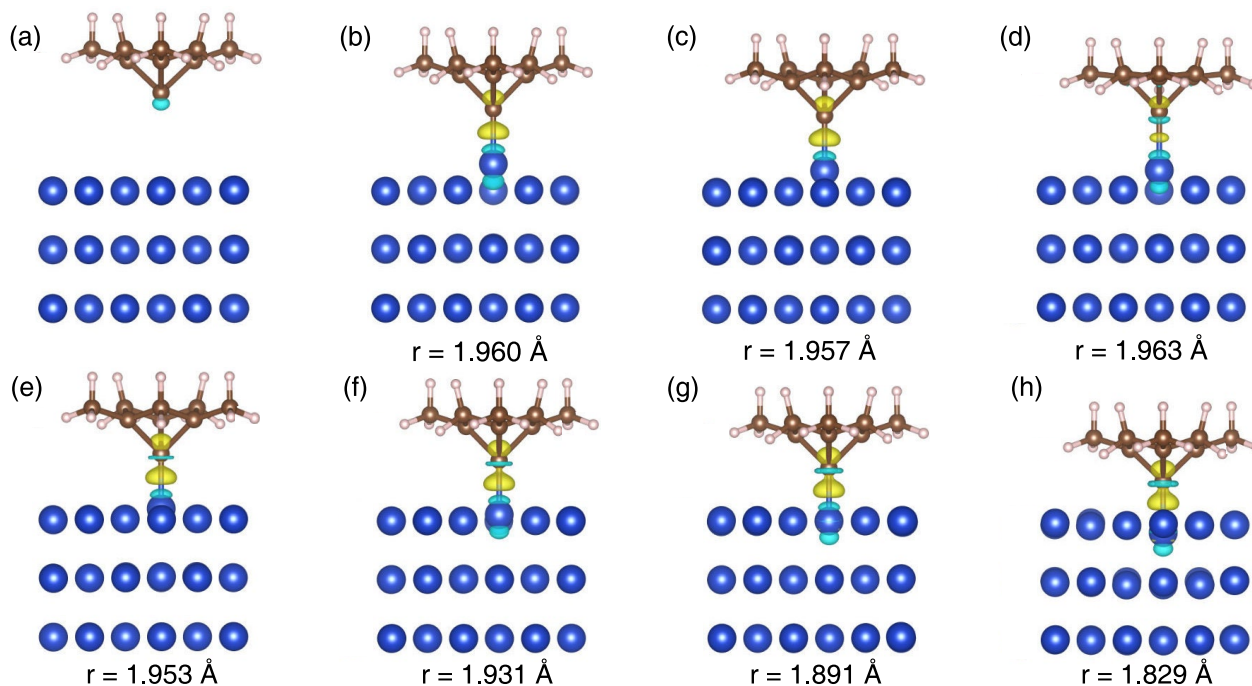


Fig. 4 CDDs (isosurface level=0.01) and C–Cu bond lengths (r) at the distances of **a** 3.5 Å, **b** 3 Å, **c** 2.8 Å, **d** 2.6 Å, **e** 2.4 Å, **f** 2.2 Å, **g** 1.9 Å, and **h** 1.4 Å

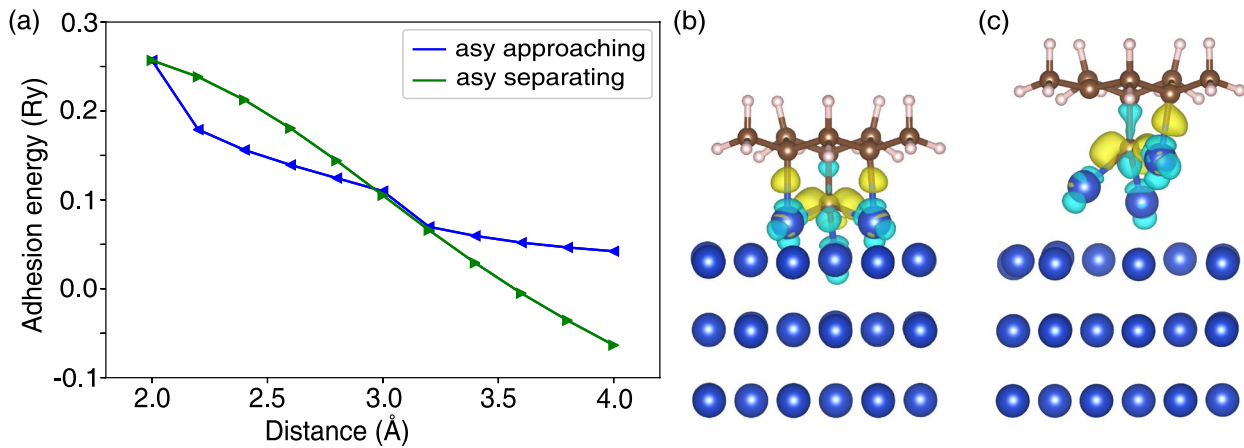


Fig. 5 a Adhesion energies during tip approaching and separating for model I on the asy site. CDDs for the ensemble with the tips on the asy sites at the distance of **b** 2 Å during indentation, and **c** 4 Å after separating (isosurface value at 0.01)

distance decreased to a distance with maximum adhesion (2.2 Å), the atom would be pulled up and then placed back on the surface. As the distance further decreased to a certain distance (1.4 Å), the atom would be pressed against the surface, but the covalent bond remained between the tip and slab. In addition, when the tip–slab distance was reduced to 2.6 Å, the covalent bonding interaction was weakened despite the increased adhesion energy. This result was demonstrated by an elongation of the covalent bond at a distance and a reduction of volume for the electron gain (Fig. 4). At this distance, the bonding Cu atom was close to its original lattice position, and the attraction between the bonding Cu atom and second-layer Cu atom was strong that the C–Cu bond was elongated. This phenomenon demonstrates the complexity at the tip–slab interface, which indicates that the “jump” and “return” of the surface atom could affect the adhesion. The real determinants of adhesion can only be the lattice structure and electronic structure at the tip–slab interface. The above-mentioned discussions are based on the calculations using a simplified tip model, which is relatively thin, thereby not allowing for greater lattice deformation. However, this phenomenon could still occur because of a large difference in bonding strengths between diamond and copper.

The following conclusions are drawn for the nanoindentation between an atomic sharp tip and a copper slab. When a diamond tip approaches the Cu (111) surface, the structural change could occur on the top site even before the actual contact because of the formation of covalent bonds, which would cause a rapid increase in adhesion strength. In addition, the tip–slab adhesion did not depend entirely on the C–Cu covalent bond strength but also on the lattice structure at the interface. These findings, normally neglected in previous studies, could affect machining. For example, the

atomic jump and return might influence the creation of surface defects and the onset of dislocation nucleation.

4.4 Adhesion for the Tip on Non-High-Symmetry Sites

The above-mentioned relaxation occurred at high-symmetry sites, and almost no lateral force was exerted on the tip during an initial-stage indentation. If the diamond tip was placed above other positions on the surface, then the tip–sample interaction could cause more complex atomic behavior, including bond rotation and breakage. Similarly, a group of simulations was conducted for tip indentation and separation on an asymmetrical site (asy site in Fig. 3) to calculate adhesion energies at different distances, and the results are shown in Fig. 5a.

As the indentation proceeded, the adhesion energy increased gradually until the distance of 2 Å, where C–C bonds broke. The relaxation process suggests that the bond breakage was due to the uneven attraction of surface copper atoms to the apex atom at this distance. The asymmetrical force exerted on the apex drove the tip atom toward a lateral direction rather than into the copper slab. As the tip moved toward the slab, the interfacial atomic structure was not at a minimum energy status and tended to form a more stable structure. Eventually, C–C bonds broke, and more C–Cu covalent bonds were formed at the tip–sample interface. This process led to an increase in adhesion energy and a complex interface structure (Fig. 5b).

Figure 5c also indicates that the strong adhesion at the interface could lead to material transfer from the substrate surface to the tip and leave atomic defects on the copper surface. Upon retraction following indentation, the surface atoms would be attached to the tip, thereby

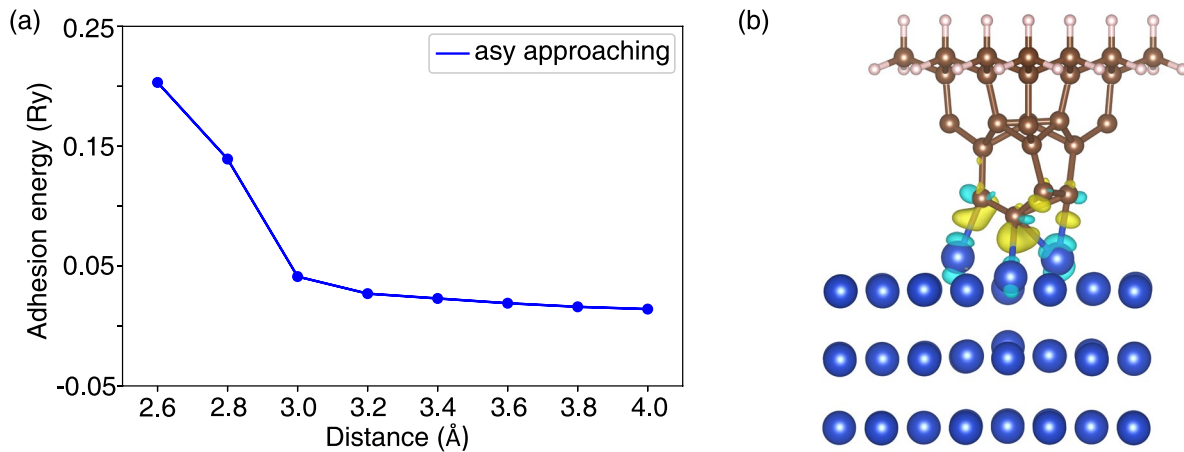


Fig. 6 **a** Adhesion energies during tip approaching for the model II on asy site. **b** CDD for model II at a distance of 2.6 Å (isosurface value at 0.01)

contaminating the diamond tip. From an electronic point of view, a contaminated tip resulted in weaker adhesion than a perfect tip because covalent bonding, which induced adhesion between the tip and slab, was compromised when attached copper atoms occupied dangling bonds on the tip.

For comparison, model II was used for indentation simulation, and the results are shown in Fig. 6. Given the surface reconfiguration on the tip, more atoms and dangling bonds exist near the apex, which allows the formation of more C–Cu bonds at the interface during contact. In addition, the presence of more C layers allows more lattice deformation. Consequently, a complex atomic structure was formed at the C–Cu interface when more C–C bonds on the tip underwent a large degree of rotation.

Considering that diamond is harder than copper, this result is surprising. An initial-stage indentation is enough to induce changes in bonds on the diamond surface and cause tool contamination. The changes in the interfacial atomic structure could lead to different tool–work adhesion energy and force. It is worth noting that our simulations only describe indentations at a shallow depth, whereas in real experiments more complex bonding interactions and atomic structures will exist at the tool–work interface.

5 Conclusions

In this paper, the tip–slab adhesion was studied using the first-principles method to reveal its nature and atomic-scale effects during nanoindentation. Based on quantum mechanical principles and atomic structure analysis, this method provided a detailed description of the adhesion between a diamond tool and a copper substrate. This method can be

extended to more cases to reveal the interfacial features of ACSM processes, even for a system with different materials and additional features through effective simulation approaches.

The modeling in this paper was at a small scale, which only considered a pure-atomic contact between a clean diamond tip and a copper surface because of computational limits. However, the DFT calculation allowed more insights into chemical bonding interactions and their effects. First, the nature of tip–slab interactions was investigated through a series of first-principles simulations. The analysis of CDDs and PDOSs showed that the adhesion was primarily from the covalent bonding interaction caused by the hybridization of C-2*p* and Cu-3*d* orbitals. The effect of tip position and angle on adhesion was also studied. The result showed that the tip at different high-symmetry sites would cause different adhesion energies and structural changes. When a tip approaches the copper surface, the structural change could occur before the actual tip–slab contact on the top site and the angular relationship between the tip and target lattice could lead to different adhesion energies on the fcc and hcp sites. Therefore, adhesion is highly sensitive to the details of lattice structure at the tip–slab interface, and even a difference of a few angstroms will lead to different adhesion effects and can further influence the formation and development of point defects or dislocations during machining. Bond rotation and breakage and its effects were discussed, and the mechanism could explain the onset of tip contamination or wear during nanoindentation. The first-principles method can describe complex atomic and electronic behavior during an initial stage of nanoindentation, which has important implications for the fabrication of atomic-scale patterns and for process control, making the quantum mechanics-based simulation a necessary approach for the fundamental study of the ACSM process.

Supplementary Information The online version contains supplementary material available at <https://doi.org/10.1007/s41871-022-00149-3>.

Acknowledgements The authors would like to thank EPSRC (EP/K018345/1, EP/T024844/1, EP/V055208/1), the Royal Society-NSFC international exchange programme (IECNSFC\181474) and Science and Technology Based for Equipment Design and Manufacturing for Introduction Talents of Discipline to Universities 2.0 of the 111 project (Project No. BP0719002) for providing financial support to this research. The authors also acknowledge the use of the EPSRC (EP/K000586/1)-funded ARCHIE-West High-Performance Computer at the University of Strathclyde.

Availability of Data and Materials The data underpinning this publication are openly available from the University of Strathclyde Knowledge Base at <https://doi.org/10.15129/8623a376-5f47-4cca-953e-9567c5b2cf63>.

Declarations

Conflict of interest On behalf of all authors, the corresponding author states that there are no conflicts of interest.

Open Access This article is licensed under a Creative Commons Attribution 4.0 International License, which permits use, sharing, adaptation, distribution and reproduction in any medium or format, as long as you give appropriate credit to the original author(s) and the source, provide a link to the Creative Commons licence, and indicate if changes were made. The images or other third party material in this article are included in the article's Creative Commons licence, unless indicated otherwise in a credit line to the material. If material is not included in the article's Creative Commons licence and your intended use is not permitted by statutory regulation or exceeds the permitted use, you will need to obtain permission directly from the copyright holder. To view a copy of this licence, visit <http://creativecommons.org/licenses/by/4.0/>.

References

- Fang F (2020) Atomic and close-to-atomic scale manufacturing: perspectives and measures. *Int J Extreme Manuf* 2:030201. <https://doi.org/10.1088/2631-7990/aba495>
- Fang F, Zhang N, Guo D et al (2019) Towards atomic and close-to-atomic scale manufacturing. *Int J Extreme Manuf* 1:012001. <https://doi.org/10.1088/2631-7990/ab0dfc>
- Hasan RMdM, Luo X (2018) Promising lithography techniques for next-generation logic devices. *Nanomanufacturing Metrol* 1:67–81. <https://doi.org/10.1007/s41871-018-0016-9>
- Mathew PT, Rodriguez BJ, Fang F (2020) Atomic and close-to-atomic scale manufacturing: a review on atomic layer removal methods using atomic force microscopy. *Nanomanufacturing Metrol* 3:167–186. <https://doi.org/10.1007/s41871-020-00067-2>
- Chang S, Geng Y, Yan Y (2022) Tip-based nanomachining on thin films: a mini review. *Nanomanufacturing Metrol* 5:2–22. <https://doi.org/10.1007/s41871-021-00115-5>
- Tseng AA (2011) Advancements and challenges in development of atomic force microscopy for nanofabrication. *Nano Today* 6:493–509. <https://doi.org/10.1016/j.nantod.2011.08.003>
- Custance O, Perez R, Morita S (2009) Atomic force microscopy as a tool for atom manipulation. *Nat Nanotechnol* 4:803–810. <https://doi.org/10.1038/nnano.2009.347>
- Sugimoto Y, Pou P, Custance O et al (2008) Complex patterning by vertical interchange atom manipulation using atomic force microscopy. *Science* 322:413–417. <https://doi.org/10.1126/science.1160601>
- Gao J, Luo X, Fang F, Sun J (2021) Fundamentals of atomic and close-to-atomic scale manufacturing: a review. *Int J Extreme Manuf* 4:012001. <https://doi.org/10.1088/2631-7990/ac3bb2>
- Sugimoto Y, Jelinek P, Pou P et al (2007) Mechanism for room-temperature single-atom lateral manipulations on semiconductors using dynamic force microscopy. *Phys Rev Lett* 98:106104. <https://doi.org/10.1103/PhysRevLett.98.106104>
- Jarvis S, Sweetman A, Bamidele J et al (2012) Role of orbital overlap in atomic manipulation. *Phys Rev B Condens Matter Mater Phys* 85:1–5. <https://doi.org/10.1103/PhysRevB.85.235305>
- Tavazza F, Levine LE (2016) DFT investigation of early stages of nanoindentation in Ni. *J Phys Chem C* 120:13249–13255. <https://doi.org/10.1021/acs.jpcc.6b01148>
- Tavazza F, Senftle TP, Zou C et al (2015) Molecular dynamics investigation of the effects of tip-substrate interactions during nanoindentation. *J Phys Chem C* 119:13580–13589. <https://doi.org/10.1021/acs.jpcc.5b01275>
- Sanna S, Dues C, Schmidt WG (2015) Modeling atomic force microscopy at LiNbO₃ surfaces from first-principles. *Comput Mater Sci* 103:145–150. <https://doi.org/10.1016/j.commatsci.2015.03.025>
- Tsugawa K, Noda H, Hirose K, Kawarada H (2010) Schottky barrier heights, carrier density, and negative electron affinity of hydrogen-terminated diamond. *Phys Rev B* 81:045303. <https://doi.org/10.1103/PhysRevB.81.045303>
- Luo X, Tong Z, Liang Y (2014) Investigation of the shape transferability of nanoscale multi-tip diamond tools in the diamond turning of nanostructures. *Appl Surf Sci* 321:495–502. <https://doi.org/10.1016/j.apsusc.2014.10.052>
- Wang Z, Luo X, Liu H et al (2021) A high-frequency non-resonant elliptical vibration-assisted cutting device for diamond turning microstructured surfaces. *Int J Adv Manuf Technol* 112:3247–3261. <https://doi.org/10.1007/s00170-021-06608-3>
- Xie W, Fang F (2019) Cutting-based single atomic layer removal mechanism of monocrystalline copper: atomic sizing effect. *Nanomanufacturing Metrol* 2:241–252. <https://doi.org/10.1007/s41871-019-00045-3>
- Zhu P, Fang F (2016) Study of the minimum depth of material removal in nanoscale mechanical machining of single crystalline copper. *Comput Mater Sci* 118:192–202. <https://doi.org/10.1016/j.commatsci.2016.03.023>
- Wang Z, Zhang J, Li G et al (2020) Anisotropy-related machining characteristics in ultra-precision diamond cutting of crystalline copper. *Nanomanufacturing Metrol* 3:123–132. <https://doi.org/10.1007/s41871-020-00060-9>
- Zhao S, Zhang Z, Wu Z et al (2019) The impacts of adhesion on the wear property of graphene. *Adv Mater Interfaces* 6:1900721. <https://doi.org/10.1002/admi.201900721>
- Shimizu J, Eda H, Zhou L, Okabe H (2008) Molecular dynamics simulation of adhesion effect on material removal and tool wear in diamond grinding of silicon wafer. *Tribol Online* 3:248–253. <https://doi.org/10.2474/trol.3.248>
- Bian R, He N, Ding W, Liu S (2017) A study on the tool wear of PCD micro end mills in ductile milling of ZrO₂ ceramics. *Int J Adv Manuf Technol* 92:2197–2206. <https://doi.org/10.1007/s00170-017-0242-0>
- Jiang G, Jianguo Z, Yanan P et al (2020) A critical review on the chemical wear and wear suppression of diamond tools in diamond cutting of ferrous metals. *Int J Extreme Manuf* 2:012001. <https://doi.org/10.1088/2631-7990/ab5d8f>

25. Song J, Srolovitz DJ (2008) Mechanism for material transfer in asperity contact. *J Appl Phys* 104:124312. <https://doi.org/10.1063/1.3043582>
26. Giannozzi P, Barone A, Bonfà P et al (2020) Quantum ESPRESSO toward the exascale. *J Chem Phys* 152:154105. <https://doi.org/10.1063/5.0005082>
27. Giannozzi P, Baroni S, Bonini N et al (2009) QUANTUM ESPRESSO: a modular and open-source software project for quantum simulations of materials. *J Phys Condens Matter* 21:395502. <https://doi.org/10.1088/0953-8984/21/39/395502>
28. Perdew JP, Burke K, Ernzerhof M (1996) Generalized gradient approximation made simple. *Phys Rev Lett* 77:3865–3868. <https://doi.org/10.1103/PhysRevLett.77.3865>
29. Prandini G, Marrazzo A, Castelli IE et al (2018) Precision and efficiency in solid-state pseudopotential calculations. *Npj Comput Mater* 4:72. <https://doi.org/10.1038/s41524-018-0127-2>
30. Pérez R, Payne MC, Štich I, Terakura K (1997) Role of covalent tip–surface interactions in noncontact atomic force microscopy on reactive surfaces. *Phys Rev Lett* 78:678–681. <https://doi.org/10.1103/PhysRevLett.78.678>
31. Liu Z, Zheng S, Lu Z et al (2018) Adhesive transfer at copper/diamond interface and adhesion reduction mechanism with fluorine passivation: a first-principles study. *Carbon* 127:548–556. <https://doi.org/10.1016/j.carbon.2017.11.027>
32. Xie H, Chen Y, Zhang T et al (2020) Adhesion, bonding and mechanical properties of Mo doped diamond/Al (Cu) interfaces: a first-principles study. *Appl Surf Sci* 527:146817. <https://doi.org/10.1016/j.apsusc.2020.146817>
33. Gross L, Mohn F, Moll N et al (2009) The chemical structure of a molecule resolved by atomic force microscopy. *Science* 325:1110–1114. <https://doi.org/10.1126/science.1176210>
34. Yurtsever A, Sugimoto Y, Tanaka H et al (2013) Force mapping on a partially H-covered Si(111)-(7 × 7) surface: Influence of tip and surface reactivity. *Phys Rev B* 87:155403. <https://doi.org/10.1103/PhysRevB.87.155403>
35. Oyabu N, Pou P, Sugimoto Y et al (2006) Single atomic contact adhesion and dissipation in dynamic force microscopy. *Phys Rev Lett* 96:106101. <https://doi.org/10.1103/PhysRevLett.96.106101>
36. Momma K, Izumi F (2011) VESTA 3 for three-dimensional visualization of crystal, volumetric and morphology data. *J Appl Crystallogr* 44:1272–1276. <https://doi.org/10.1107/S0021889811038970>
37. Feldbauer G, Wolloch M, Bedolla PO et al (2015) Adhesion and material transfer between contacting Al and TiN surfaces from first principles. *Phys Rev B* 91:165413. <https://doi.org/10.1103/PhysRevB.91.165413>
38. Luan B, Robbins MO (2005) The breakdown of continuum models for mechanical contacts. *Nature* 435:929–932. <https://doi.org/10.1038/nature03700>
39. Cross G, Schirmeisen A, Stalder A et al (1998) Adhesion interaction between atomically defined tip and sample. *Phys Rev Lett* 80:4685–4688. <https://doi.org/10.1103/PhysRevLett.80.4685>
40. Giessibl FJ, Herz M, Mannhart J (2002) Friction traced to the single atom. *Proc Natl Acad Sci* 99:12006–12010. <https://doi.org/10.1073/pnas.182160599>
41. Lantz MA (2001) Quantitative measurement of short-range chemical bonding forces. *Science* 291:2580–2583. <https://doi.org/10.1126/science.1057824>
42. Loppacher C, Bennewitz R, Pfeiffer O et al (2000) Experimental aspects of dissipation force microscopy. *Phys Rev B* 62:13674–13679. <https://doi.org/10.1103/PhysRevB.62.13674>
43. Sugimoto Y (2016) Atomic force microscopy for imaging, identification and manipulation of single atoms. *E-J Surf Sci Nanotechnol* 14:28–34. <https://doi.org/10.1380/ejssnt.2016.28>
44. Qi Y, Konca E, Alpas AT (2006) Atmospheric effects on the adhesion and friction between non-hydrogenated diamond-like carbon (DLC) coating and aluminum – a first-principles investigation. *Surf Sci* 600:2955–2965. <https://doi.org/10.1016/j.susc.2006.05.008>
45. Monkhorst HJ, Pack JD (1976) Special points for Brillouin-zone integrations. *Phys Rev B* 13:5188–5192. <https://doi.org/10.1103/PhysRevB.13.5188>
46. Paul E, Evans CJ, Polvanit RS (1996) Chemical aspects of tool wear in single point diamond turning. *Precis Eng* 18:16. [https://doi.org/10.1016/0141-6359\(95\)00019-4](https://doi.org/10.1016/0141-6359(95)00019-4)